Novel Pre-compensation Schemes for Low-Cost Nonlinear Tera-Hertz Transmitters

Yahia R. Ramadan, Mahmoud E. Abdelgelil, and Hlaing Minn
Electrical and Computer Engineering Department, The University of Texas at Dallas
Email: {yahia.ramadan, mahmoud.abdelgelil, hlaing.minn}@utdallas.edu

***Abstract*—Tera-Hertz (THz) transmission can offer several attractive applications, yet developing low-cost energy-efficient THz devices is at an early stage. The most promising low-cost THz transmitter architecture in the literature is the so-called frequency-multiplier-last architecture but it is incapable of transmitting quadrature amplitude modulation (QAM) due to the architecture's inherent nonlinear distortions. We study such nonlinear THz communication systems by incorporating the nonlinearity aspects of the low-cost THz devices into the signal model. Then we propose novel pre-compensation schemes to compensate the nonlinearity effect, thus enabling QAM-capable frequency-multiplier-last architecture for THz systems. Numerical results show that the proposed pre-compensation schemes overcome the prominent problems experienced in the existing scheme, namely severe nonlinear distortions of the modulation symbols as well as spectral spreading and/or large spectrum sidelobes.**

***Index Terms*—Low-cost, nonlinear transceivers, nonlinear distortion, pre-compensation, QAM, terahertz.**

I. Introduction

The tera-hertz (THz) band is one of the least explored areas. It exhibits unique features unavailable in the frequency bands of current and near-future communication systems. It can accommodate detection of specific types of gaseous molecules in targeted environments, thus enabling various applications including breath analysis for non-invasive medical diagnosis and indoor/industrial air quality control [1]–[9]. The THz band offers substantially larger bandwidth and data rates not feasible in the current and 5G communication systems, thus the IEEE 802.15 Task Group 3d is developing a THz communication standard for applications such as wireless kiosks for multimedia and software download, small-cells wireless fronthaul and backhaul, and for data centers. The small form-factor of THz circuits also enables chip-to-chip or within-device communications and enhanced beamforming for physical layer security of wireless communications. These advantages are very attractive but for broader consumer applications the major barrier is the cost of THz devices. There remain several technical challenges for low-cost applications.

Signal generation circuitries for low-cost THz devices are different from the conventional ones of the lower frequency bands. This is due to unavailability of THz oscillators and THz CMOS power amplifiers which is commonly known as "the THz Gap" [10]. Thus, low-cost THz transceivers rely on nonlinear devices in contrast to the linear devices of the lower frequency bands. Another crucial limitation of low-cost THz devices is the output power constraint which has a direct effect on the sensing/communication range and performance. There are a few low-cost state-of-the-art CMOS THz transmitter architectures in the recent literature. The two most promising ones are the so-called frequency-multiplier-last architecture from the UC-Berkeley [11], [12] and the cubic mixer architecture from Japan [13], [14]. The former [11] has an advantage of 14.5dB higher output power and 8 dB lower DC power consumption than the latter. However, the frequency-multiplier-last architecture [11], [12] is not capable of transmitting quadrature amplitude modulation (QAM) schemes while the mixer architecture [13], [14] is. The research group of the latter also developed a doubler mixer architecture in [15] which yields a higher output power due to the use of doubler rather than tripler. This paper focuses on the frequency-multiplier-last architecture since it has substantial advantages in terms of transmitter output power and DC power consumption which are much needed to address the propagation range limitation and energy efficiency. The major limitations/challenges of the frequency-multiplier-last architecture reported in the recent literature are its incapability with QAM and its undesired spectrum spreading, both due to nonlinear distortions. These nonlinear distortions impose new fundamental challenges for designing reliable and efficient communications systems in the nonlinear regime.

If compared to the existing communication systems, THz communication introduces several challenges including communication range limitation, distance and frequency dependent channel characteristics, and more difficult synchronization, equalization and distortion compensation [16]. When low cost constraint (i.e., CMOS device) is imposed, the most energy-efficient transmitter architecture in the literature [11] causes an additional challenge of nonlinear distortion to the message signals which prevents reliable transmission of QAM signals. Communication theory in such nonlinear systems has not been investigated in the literature and we address it in this paper.

In this paper, we study such nonlinear THz communication system by incorporating the nonlinearity aspects of the low-cost THz devices in the signal model. We show that without pre-compensation and with pulse shaping filter spanning more than one symbol, the transmitter output constellation experiences significant distortions. In addition, the existing frequency-multiplier-last architecture is not capable of transmitting QAM. Therefore, we propose novel pre-compensation schemes to compensate the nonlinearity effect and enable low-cost THz QAM transmission. Numerical results show that the proposed pre-compensation schemes can effectively handle severe nonlinear distortions and spectrum spreading issues of the low-cost frequency-multiplier-last THz transmitter.

978-1-5386-3180-5/18/$31.00 ©2018 IEEE

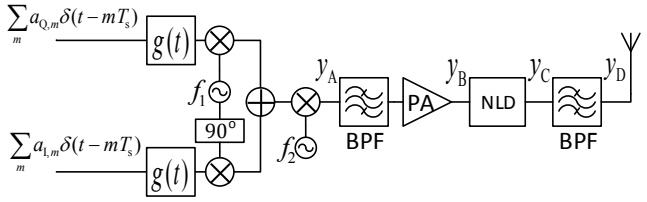

Fig. 1. Frequency-multiplier-last transmitter architecture for IQ transmission [11]. (BPF = bandpass filter, PA = power amplifier, NLD = nonlinear device)

The rest of the paper is organized as follows. In section II, we describe the system model and derive an accurate signal model. In section III, we introduce the proposed pre-compensation schemes. Numerical results are presented in section IV. Finally, section V concludes the paper.

II. System and Signal Model

In order to investigate the effect of nonlinear THz transmitters, we consider a single-antenna THz communication system. The extension to multi-antenna systems can be straightly done. The transmitter utilizes the frequency-multiplier-last architecture [11] for an in-phase and quadrature (IQ) transmission as shown in Fig. 1. The frequency multiplier block is implemented by a nonlinear device followed by filtering, and it is the source of nonlinear distortion. The modulation signals for the I and Q branches can be given by

$$s_\mathrm{I}(t) = \sum_m a_{\mathrm{I},m}\delta(t - mT_\mathrm{s}), \tag{1}$$

$$s_\mathrm{Q}(t) = \sum_m a_{\mathrm{Q},m}\delta(t - mT_\mathrm{s}), \tag{2}$$

where $a_m \triangleq a_{\mathrm{I},m} + ja_{\mathrm{Q},m}$ is a modulation symbol and T_s is the symbol duration. With a pulse-shaping filter $g(t)$, the baseband signal $\tilde{s}(t) = \tilde{s}_\mathrm{I}(t) + j\tilde{s}_\mathrm{Q}(t)$ is given by $\tilde{s}_\mathrm{I}(t) = s_\mathrm{I}(t) * g(t)$ and $\tilde{s}_\mathrm{Q}(t) = s_\mathrm{Q}(t) * g(t)$, where $*$ denotes the convolution operation. Then, after some manipulations, the signal $y_\mathrm{A}(t)$ at the output of the mixer with frequency f_2 is given by

$$\begin{aligned} y_\mathrm{A}(t) =& \alpha\tilde{s}_\mathrm{I}(t)\big[\cos(2\pi f_3 t) + \cos(2\pi f_4 t)\big] \\ &- \alpha\tilde{s}_\mathrm{Q}(t)\big[\sin(2\pi f_3 t) - \sin(2\pi f_4 t)\big] \end{aligned} \tag{3}$$

where $f_3 = f_2 + f_1$, $f_4 = f_2 - f_1$, and α is a scaling parameter. The bandpass filter (BPF) allows the desired signal around f_3 and suppresses other terms, thus the signal $y_\mathrm{B}(t)$ at the input of the nonlinear device (NLD) becomes

$$y_\mathrm{B}(t) = \alpha\tilde{s}_\mathrm{I}(t)\cos(2\pi f_3 t) - \alpha\tilde{s}_\mathrm{Q}(t)\sin(2\pi f_3 t). \tag{4}$$

We consider a polynomial model for the NLD (i.e., for an input x, the output is $\sum_{k=1}^{K} A_k x^k$). The larger order terms typically have smaller coefficients but their spectrum spreadings are wider. Thus, the choice of f_1 and f_2 should be properly chosen to avoid/control interferences of higher order terms on the desired nonlinear term. Furthermore, larger order terms may introduce some floor of distortions. The NLD used in the THz transmitter typically has a differential output, and hence even order terms will be canceled. Therefore, the nonlinear device output signal $y_\mathrm{C}(t)$ is given by

$$\begin{aligned} y_\mathrm{C}(t) =& A_1\alpha\left(\tilde{s}_\mathrm{I}(t)\cos(2\pi f_3 t) - \tilde{s}_\mathrm{Q}(t)\sin(2\pi f_3 t)\right) \\ &+ A_3\alpha^3\left(\tilde{s}_\mathrm{I}(t)\cos(2\pi f_3 t) - \tilde{s}_\mathrm{Q}(t)\sin(2\pi f_3 t)\right)^3 \\ &+ A_5\alpha^5\left(\tilde{s}_\mathrm{I}(t)\cos(2\pi f_3 t) - \tilde{s}_\mathrm{Q}(t)\sin(2\pi f_3 t)\right)^5 + \ldots. \end{aligned} \tag{5}$$

If we consider the desired signal to be centered around a THz carrier $f_\mathrm{T} = 3f_3$, it will be contributed mainly by $(\cdot)^3$ and partially by $(\cdot)^5$. The last BPF allows the desired signal centered around the THz carrier f_T and suppresses other terms, yielding $y_\mathrm{D}(t)$ shown at the bottom of the page. The equivalent lowpass signal of $y_\mathrm{D}(t)$ is $x_\mathrm{BB}(t) = x_\mathrm{I}(t) + jx_\mathrm{Q}(t)$. We can observe that the nonlinearity modifies the baseband signal $\tilde{s}(t)$ into $x_\mathrm{BB}(t)$ as

$$\begin{aligned} x_\mathrm{BB}(t) =& \frac{A_3\alpha^3}{4}\tilde{s}^3(t) + \frac{5A_5\alpha^5}{16}\big(\tilde{s}_\mathrm{I}^5(t) - 3\tilde{s}_\mathrm{I}(t)\tilde{s}_\mathrm{Q}^4(t) - 2\tilde{s}_\mathrm{I}^3(t)\tilde{s}_\mathrm{Q}^2(t) \\ &+ j\big(2\tilde{s}_\mathrm{I}^2(t)\tilde{s}_\mathrm{Q}^3(t) + 3\tilde{s}_\mathrm{I}^4(t)\tilde{s}_\mathrm{Q}(t) - \tilde{s}_\mathrm{Q}^5(t)\big)\big), \end{aligned} \tag{7}$$

which causes nonlinear distortions of modulation symbols as well as spectral spreading and larger spectrum sidelobes.

III. Proposed Pre-Compensation Schemes

An important entity which influences the nonlinear distortions of the frequency-multiplier architecture is the transmit baseband pulse-shaping filter before the frequency multiplier. For low-cost THz transmitters, the filtering after the frequency multiplier circuit is implemented by means of on-chip connection line and on-chip antenna, and hence the filtering performance at that stage is rather loose. Thus, the role of the baseband pulse-shaping filter is more prominent for controlling output power spectrum. Differences from the existing lower band systems are complications due to nonlinearity of the frequency multiplier and the loose filtering after the frequency multiplier.

Recent literature demonstrated feasibility of quadrature phase-shift keying (QPSK) in such nonlinear systems [11] where the message points in the QPSK constellation just experience a predefined permutation. However, we note that these results are valid only if the baseband pulse-shaping filter impulse response is limited within one symbol interval (T_s) which causes high level of spectrum sidelobes. To keep adjacent channel interferences at an acceptable level, the spectrum sidelobes need to be substantially lowered which requires the use of a larger span of the pulse-shaping filter. To illustrate

$$\begin{aligned} y_\mathrm{D}(t) =& \underbrace{\left[\frac{A_3\alpha^3}{4}\left(\tilde{s}_\mathrm{I}^3(t) - 3\tilde{s}_\mathrm{I}(t)\tilde{s}_\mathrm{Q}^2(t)\right) + \frac{5A_5\alpha^5}{16}\left(\tilde{s}_\mathrm{I}^5(t) - 3\tilde{s}_\mathrm{I}(t)\tilde{s}_\mathrm{Q}^4(t) - 2\tilde{s}_\mathrm{I}^3(t)\tilde{s}_\mathrm{Q}^2(t)\right)\right]}_{x_\mathrm{I}(t)}\cos(2\pi f_\mathrm{T} t) \\ &- \underbrace{\left[\frac{A_3\alpha^3}{4}\left(3\tilde{s}_\mathrm{I}^2(t)\tilde{s}_\mathrm{Q}(t) - \tilde{s}_\mathrm{Q}^3(t)\right) + \frac{5A_5\alpha^5}{16}\left(2\tilde{s}_\mathrm{I}^2(t)\tilde{s}_\mathrm{Q}^3(t) + 3\tilde{s}_\mathrm{I}^4(t)\tilde{s}_\mathrm{Q}(t) - \tilde{s}_\mathrm{Q}^5(t)\right)\right]}_{x_\mathrm{Q}(t)}\sin(2\pi f_\mathrm{T} t). \end{aligned} \tag{6}$$

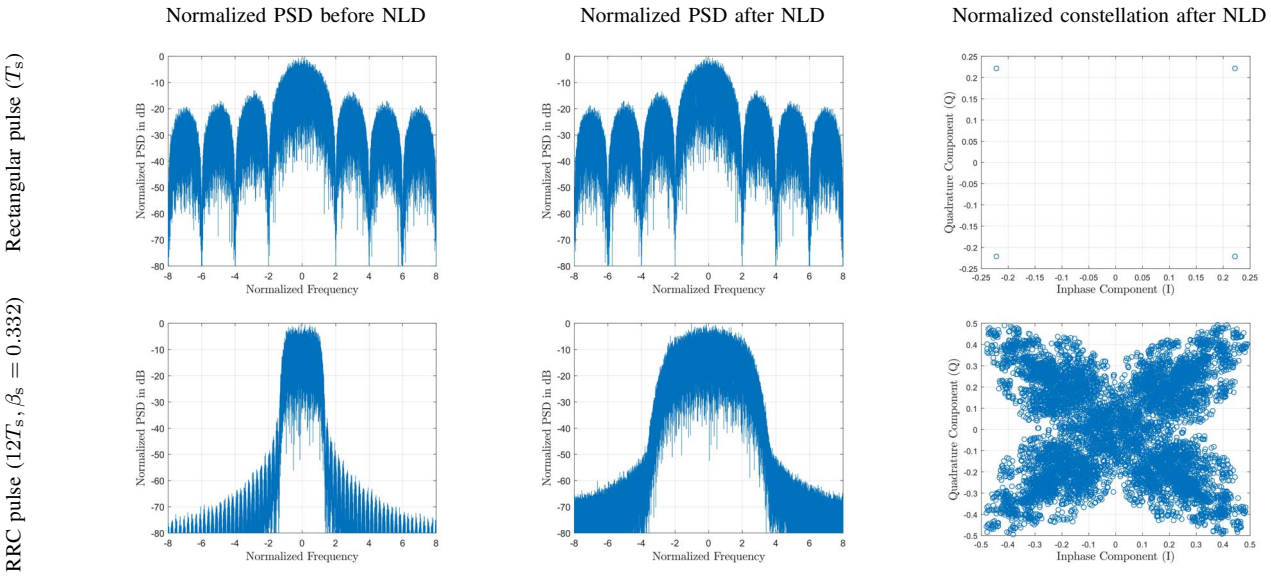

Fig. 2. Combined effect of the baseband pulse-shaping filter and the NLD on QPSK (the existing scheme in [11]). (β_s = roll-off factor)

this, for QPSK modulation, Fig. 2 shows the power spectrum density (PSD) of the signals before and after the NLD and the transmitter output constellation for two different pulse-shaping filters: 1) rectangular pulse-shaping filter spanning one symbol and 2) root-raised cosine (RRC) pulse-shaping filter spanning 12 symbols. We observe that a larger filter span yields a lower spectrum sidelobe but a severe degradation of the transmitter output constellation due to nonlinear distortion. This shows that new communication strategies are needed for both QPSK and QAM signals for energy and spectrum efficient low-cost THz systems.

We develop a pre-compensated signaling scheme for the frequency-multiplier which induces nonlinear distortions. Suppose for a block of M modulation symbols $\{a_m\}$, the ideal lowpass-equivalent transmitted signal without any distortion is denoted by

$$z(t) = \sum_m a_m g(t - mT_s),$$

where $g(t)$ is the desired baseband pulse-shaping filter impulse response, and $T_s = 1/R_s$ where R_s is the desired data rate. Denote the lowpass-equivalent signal of the proposed scheme before the frequency multiplier by $x(t) = \sum_k c_k q(t - kT_c)$ where T_c is the virtual sample duration, $\{c_k\}$ are virtual samples to be derived from $z(t)$, and $q(t)$ is the actual baseband pulse-shaping filter. For not so large QAM size, the contribution of the fifth order can be neglected since $A_3 \gg A_5$. Then based on the signal model in (7), the proposed scheme for the frequency tripler can be formulated as a solution to the following problem:

$$\min_{\{c_k\}, q(t), T_c} \int |z(t) - (\sum_k c_k q(t - kT_c))^3|^2 dt, \qquad (8)$$

where the integral is over the time span of the signal block. If the time span of $g(t)$ is limited to T_s, then the solution to the problem in (8) is given by $c_k = a_k^{1/3}$, $q(t) = g^{1/3}(t)$ and $T_c = T_s$. However, as mentioned earlier, for controlling adjacent channel interference, a larger filter span for $g(t)$ is needed and solving the above problem becomes more challenging.

To make the problem in (8) more tractable, we approximate it to the following problem:

$$\min_{\{c_k\}, q(t), T_c} \int |z^{1/3}(t) - (\sum_k c_k q(t - kT_c))|^2 dt. \qquad (9)$$

In a limiting sense that the squared-error function (the integrand) approaches zero, the two problems in (8) and (9) become equivalent. Now, let us consider the problem in (9) which can be viewed as finding a sampling period T_c, the discrete-time virtual samples $\{c_k\}$, and the interpolation (construction) filter $q(t)$ such that the corresponding analog signal constructed from $\{c_k\}$ will have minimum Euclidean distance to the signal $z^{1/3}(t)$. Note that the spectrum of $z(t)$ is not strictly band-limited due to the time-limited $g(t)$. Furthermore, due to the one-third order, the PSD of $z^{1/3}(t)$ is more spread than that of $z(t)$. Thus, the sampling rate $R_c = 1/T_c$ for $\{c_k\}$ should be higher than the symbol rate R_s and we consider $T_c = T_s/L$, i.e., $R_c = LR_s$, for some integer upsampling factor L. If R_c is sufficiently high enough, aliasing effect will be insignificant. Then we can obtain $\{c_k\}$ by sampling $z^{1/3}(t)$ at sampling rate R_c. In order to maintain zero error of construction (zero integrand) at time instants $\{kT_c\}$ in (9), $q(t)$ should satisfy Nyquist's zero inter-symbol interference criterion. Furthermore, $q(t)$ should preserve $\{c_k\}$ and also be independent of $\{c_k\}$. Thus, we propose to use $q(t)$ as a truncated raised cosine (RC) filter given by

$$q(t) = \frac{\operatorname{sinc}\left(\frac{t}{T_c}\right) \cos\left(\frac{\pi \beta_c t}{T_c}\right)}{1 - \left(\frac{2\beta_c t}{T_c}\right)^2}, -\frac{NT_c}{2} \le t \le \frac{NT_c}{2}, \qquad (10)$$

where $\operatorname{sinc}(x) = \sin(\pi x)/\pi x$, β_c is the roll-off factor to be determined, and N is the time span.

The proposed pre-compensated signaling scheme is shown in Fig. 3 where $\{a_{I,m} + j a_{Q,m}\}$ are QAM symbols with the symbol rate R_s. The pre-compensation block generates $\{c_{I,k}, c_{Q,k}\}$ at the rate of R_c. Also note that the pulse-shaping filter $q(t)$ in Fig. 3 has a wider bandwidth than $g(t)$ in Fig. 1.

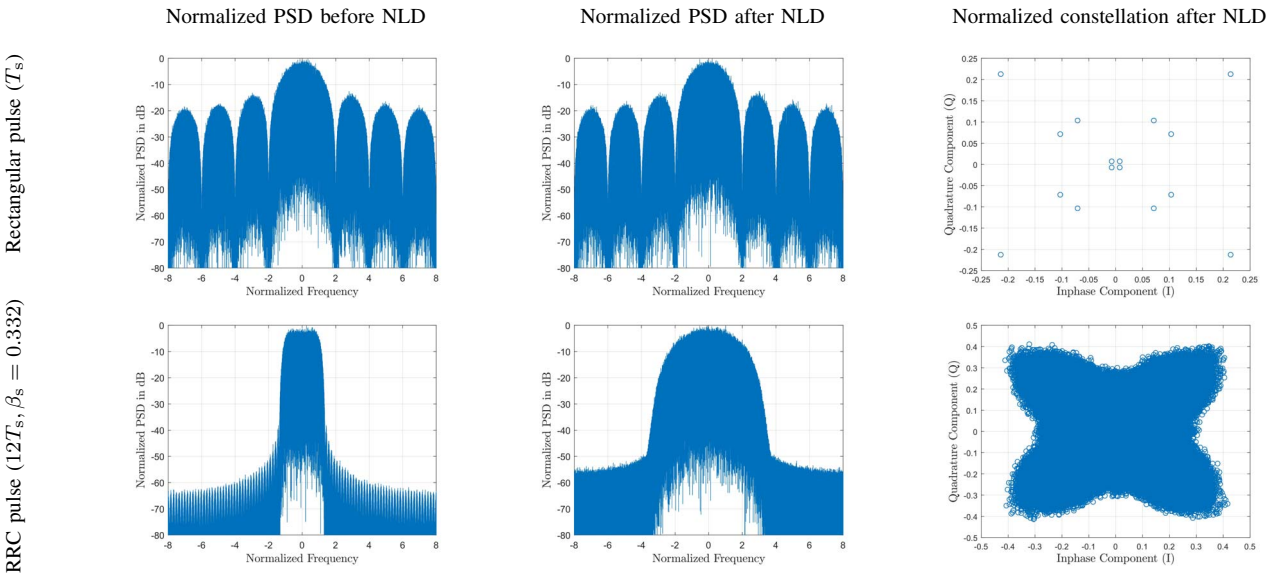

Fig. 4. Combined effect of the baseband pulse-shaping filter and the NLD on 16-QAM without pre-compensation (the existing scheme in [11]).

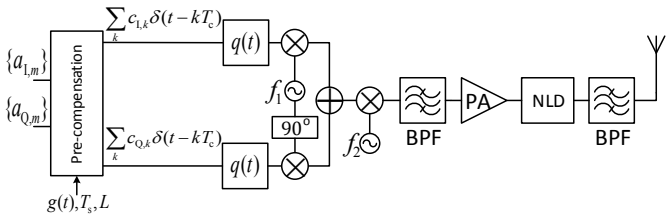

Fig. 3. Proposed pre-compensation scheme based on frequency-multiplier-last transmitter architecture for IQ transmission.

For a signal block of M QAM symbols, the proposed pre-compensation scheme generates $K = LM$ virtual samples $\{c_k\}$. For each $z(kT_c)$, there are three roots of c_k satisfying $c_k^3 = z(kT_c)$ as

$$\tilde{c}_{k,n} = |z(kT_c)|^{1/3} e^{j\left(\frac{\angle z(kT_c)}{3} + \frac{2\pi(n-2)}{3}\right)} \text{ for } n = 1, 2, 3; \ \forall k. \tag{11}$$

Therefore, we have 3^K possible virtual sequences for $\{c_k\}$. As a basic pre-compensation scheme, we generate the virtual samples by always taking the first root. As an improved pre-compensation scheme, we choose the virtual sequence having the smallest PSD spread (slowest time variation) since the samples are correlated due to the higher sampling rate R_c than the symbol rate R_s of $z(t)$. However, the exhaustive search over 3^K virtual sequences to find the optimal solution is not practically affordable for large values of K. Hence, we propose a low-complexity suboptimal algorithm to obtain the virtual sequence $\{c_k\}$ as described in Algorithm 1. The main idea of Algorithm 1 is to find the virtual samples sequentially by minimizing the Euclidean distance between each two successive virtual samples. The computational complexity of Algorithm 1 is $\mathcal{O}(3K)$.

IV. Numerical Results

We consider a desired transmitted signal $z(t)$ constructed from a block of $M = 128$ 16-QAM modulation symbols convolved with a desired pulse-shaping filter $g(t)$. Unless mentioned otherwise, we consider $g(t)$ as an RRC pulse-shaping filter with time span of $12T_s$ and roll-off factor $\beta_s = 0.332$. We generate our numerical results based on 10 000 blocks.

Algorithm 1 Proposed improved pre-compensation scheme

Inputs: $z(t)$, T_c, K
$c_1 = |z(T_c)|^{1/3} e^{j\angle|z(T_c)|/3}$
for $k = 2$ to K
  Calculate the three roots $\{\tilde{c}_{k,n}\}_{n=1}^3$ of $z(kT_c)$ using (11)
  Calculate the Euclidean distances between each of the three roots and c_{k-1}: $\{d_n = |\tilde{c}_{k,n} - c_{k-1}|^2\}$
  Find the root with minimum Euclidean distance: $\tilde{n} = \arg\min_n \{d_n\}$
  Obtain c_k as $c_k = \tilde{c}_{k,\tilde{n}}$
end for
Output: $\{c_k\}$

A. Effect of the pulse-shaping filter without pre-compensation

For illustration, we consider two types of pulse-shaping filters for $g(t)$: 1) Rectangular pulse-shaping filter with time span of T_s and 2) RRC pulse-shaping filter with time span of $12T_s$ and roll-off factor $\beta_s = 0.332$. For the existing scheme in [11] (i.e., without pre-compensation), Fig. 4 shows the PSD of the signals before and after the NLD and the transmitter output constellation. Unlike QPSK modulation with rectangular pulse-shaping which just experiences predefined permutation as shown in Fig. 2, 16-QAM modulation with rectangular pulse-shaping experiences some distortion in the transmitter output constellation. Next, comparing the results between the two pulse-shaping filters, one can observe that a larger filter span yields a lower spectrum sidelobe but a severe degradation of the transmitter output constellation due to nonlinear distortion.

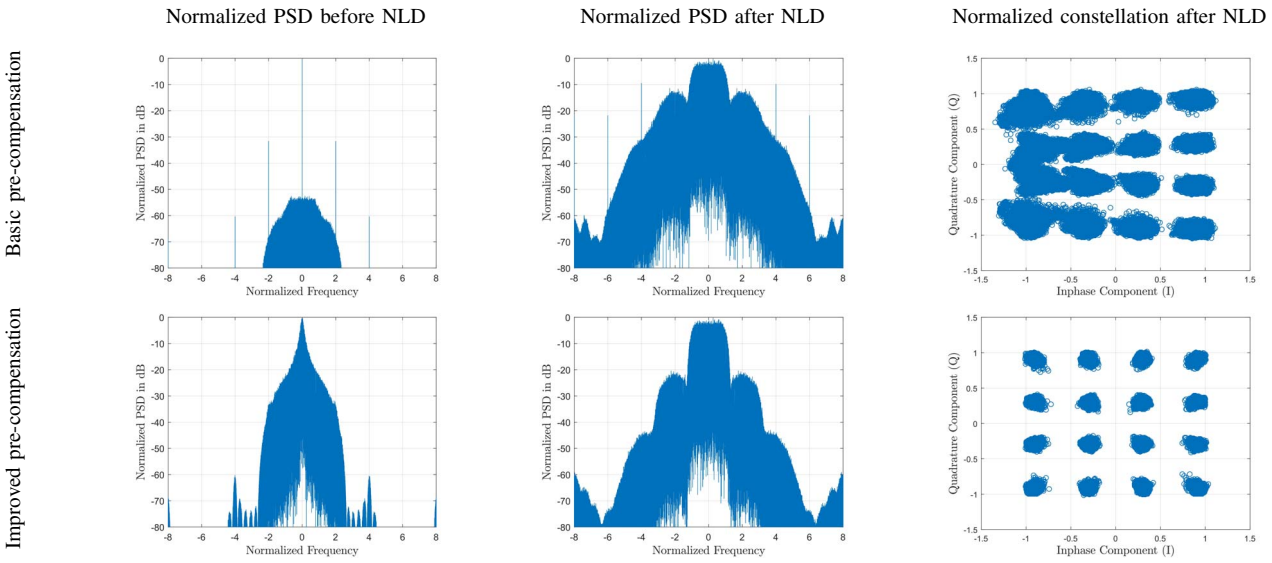

Fig. 5. Combined effect of the baseband pulse-shaping filter and the NLD on 16-QAM with the proposed pre-compensation schemes with upsampling factor $L = 2$ and RC construction filter with time span of $12T_c$ and $\beta_c = 0.332$.

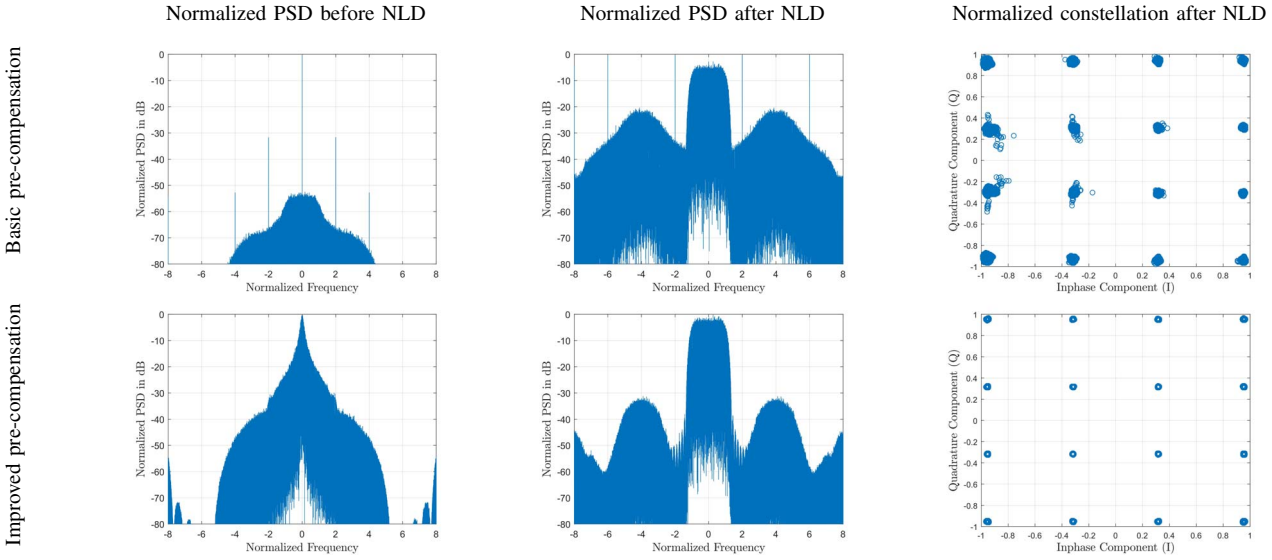

Fig. 6. Combined effect of the baseband pulse-shaping filter and the NLD on 16-QAM with the proposed pre-compensation schemes with upsampling factor $L = 4$ and RC construction filter with time span of $12T_c$ and $\beta_c = 0.332$.

B. Effect of the proposed pre-compensation schemes

Fig. 5 shows the performances of the proposed basic pre-compensation scheme (generating the virtual samples by always taking the first root) and the proposed improved pre-compensation scheme (generating the virtual samples using Algorithm 1) with upsampling factor $L = 2$ and RC construction filter $q(t)$ as in (10) with time span of $12T_c$ and roll-off factor $\beta_c = \beta_s = 0.332$. Fig. 6 extends the results of Fig. 5 to the case of upsampling factor $L = 4$. Comparing the signal constellation results of the larger filter span between the existing scheme in Fig. 4 and the proposed schemes in Fig. 5 and Fig. 6, we can clearly see performance advantages of the proposed schemes in suppressing nonlinear distortions. Compared to the proposed basic pre-compensation scheme, we observe that the proposed improved pre-compensation scheme has better PSDs (lower sidelobe levels and no spikes) before and after the NLD and less constellation distortion. This performance improvement comes from the fact that the proposed improved pre-compensation scheme in Algorithm 1 generates the virtual samples to have slower time variations, which results in a more-spectrally-constrained construction of $z^{1/3}(t)$ from the virtual samples. The proposed pre-compensation schemes with $L = 4$ yields better PSDs and less distortions than those with $L = 2$ due to its higher sampling rate LR_s which results in smaller aliasing issue and better construction for $z^{1/3}(t)$ from the virtual samples. The cost for a larger L is the increased computational complexity in the pre-compensation stage.

C. Effect of the roll-off factor of the RC construction filter

With the proposed improved pre-compensation scheme, Fig. 7 shows the normalized error vector magnitude (NEVM)

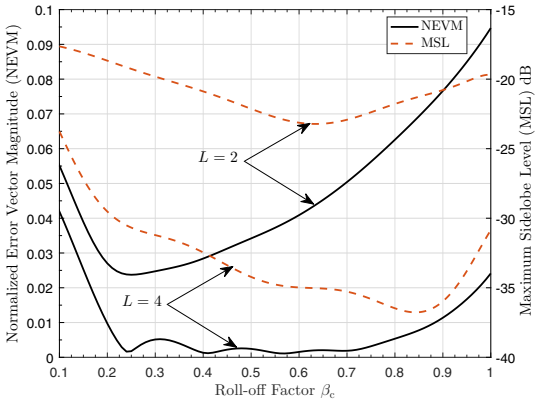

Fig. 7. NEVM and MSL versus roll-off factor β_c of the RC construction filter $q(t)$.

of transmitter output constellation[1] (left y-axis) and maximum sidelobe level (MSL) of transmitter output (right y-axis) versus the roll-off factor β_c of the RC construction filter $q(t)$ with different upsampling factor L. We observe that the minimum NEVM is not obtained along with the minimum MSL. In other words, we have a trade off between NEVM and MSL. Therefore, appropriate values for the roll-off factor β_c of the construction filter $q(t)$ and the upsampling factor L have to be determined according to the system requirements. For example, if the system requires the sidelobe level to be at most -20dB, we can select $L = 2$ for lower complexity and $\beta_c = 0.32$ which yields an NEVM of about 2.5%. If the system needs to limit its sidelobe level to be below -35dB, then we can select $L = 4$ and $\beta_c = 0.7$ which yields an NEVM of about 0.19%.

V. Conclusion

Low cost and energy efficiency are crucial factors for broader deployment of THz applications. The recently proposed frequency-multiplier-last THz transmitter architecture is the most promising one in this regard, but it suffers from nonlinear distortions and is incapable of supporting QAM transmission. In this paper, we developed solutions to overcome limitations/drawbacks of this architecture. By incorporating nonlinearity aspects of the low-cost THz devices into the signal model, our study shows that when the pulse-shaping filter spans more than one symbol, the existing result that QPSK modulation does not experience distortions except a fixed permutation of the constellation points no longer holds. For out-of-band spectrum control, the pulse-shaping filter span of several symbol intervals is needed and in this case both QPSK and QAM suffer severe nonlinear distortions. We also developed novel pre-compensation schemes which can suppress nonlinear distortions and enable QAM transmission capability. The proposed improved pre-compensation scheme offers very attractive output power spectral density control and nonlinear distortion suppression. We also presented how to tradeoff complexity and performance of the proposed scheme by means of the upsampling factor and the construction filter roll-off factor.

[1]NEVM is defined as NEVM $= \sqrt{\frac{1}{M}\sum_{m=1}^{M}|a_m - \tilde{a}_m|^2}$, where $\tilde{a}_m$ is the measured modulation symbol, and the modulation symbols $\{a_m\}$ are normalized to have average unit energy [17].

References

[1] N. Sharma, Q. Zhong, Z. Chen, W. Choi, J. P. McMillan, C. F. Neese, R. Schueler, I. Medvedev, F. D. Lucia, and K. O, "200-280 GHz CMOS RF front-end of transmitter for rotational spectroscopy," in *Proc. IEEE Symposium on VLSI Technology 2016*, June 2016, pp. 1–2.

[2] Q. Zhong, W. Choi, N. Sharma, Z. Ahmad, J. P. McMillan, C. F. Neese, F. C. D. Lucia, and K. K. O, "225-280 GHz receiver for rotational spectroscopy," in *Proc. IEEE Radio Frequency Integrated Circuits Symposium (RFIC) 2016*, May 2016, pp. 298–301.

[3] N. Sharma, J. Zhang, Q. Zhong, W. Choi, J. P. McMillan, C. F. Neese, F. C. D. Lucia, and K. O. Kenneth, "85-to-127 GHz CMOS transmitter for rotational spectroscopy," in *Proc. IEEE Custom Integrated Circuits Conference 2014*, Sept 2014, pp. 1–4.

[4] A. Nahata, A. S. Weling, and T. F. Heinz, "A wideband coherent terahertz spectroscopy system using optical rectification and electro-optic sampling," *Applied Physics Letters*, vol. 69, no. 16, pp. 2321–2323, 1996.

[5] Y. He, E. P. J. Parrott, and E. Pickwell-MacPherson, "Adaptive sampling for terahertz time-domain spectroscopy and imaging," *IEEE Trans. THz Sci. Technol.*, vol. 7, no. 2, pp. 118–123, March 2017.

[6] K. Schmalz, J. Borngraber, P. Neumaier, N. Rothbart, D. Kissinger, and H. W. Hubers, "Gas spectroscopy system at 245 and 500 GHz using transmitters and receivers in SiGe BiCMOS," in *Proc. Global Symposium on Millimeter Waves (GSMM) ESA Workshop on Millimetre-Wave Technology and Applications 2016*, June 2016, pp. 1–4.

[7] N. Rothbart, K. Schmalz, J. Borngraber, D. Kissinger, and H. W. Hubers, "Gas spectroscopy by voltage-frequency tuning of a 245 GHz SiGe transmitter and receiver," *IEEE Sensors J.*, vol. 16, no. 24, pp. 8863–8864, Dec 2016.

[8] K. Schmalz, N. Rothbart, P. F. X. Neumaier, J. Borngraber, H. W. Hubers, and D. Kissinger, "Gas spectroscopy system for breath analysis at mm-wave/THz using SiGe BiCMOS circuits," *IEEE Trans. Microw. Theory Techn.*, vol. 65, no. 5, pp. 1807–1818, May 2017.

[9] A. Tang, B. Drouin, Y. Kim, G. Virbila, and M. C. F. Chang, "95-105 GHz 352 mW all-silicon cavity-coupled pulsed echo rotational spectroscopy system in 65 nm CMOS," *IEEE Trans. THz Sci. Technol.*, vol. 7, no. 3, pp. 244–249, May 2017.

[10] V. Petrov, A. Pyattaev, D. Moltchanov, and Y. Koucheryavy, "Terahertz band communications: Applications, research challenges, and standardization activities," in *Proc. 8th International Congress on Ultra Modern Telecommunications and Control Systems and Workshops (ICUMT) 2016*, Oct 2016, pp. 183–190.

[11] S. Kang, S. V. Thyagarajan, and A. M. Niknejad, "A 240GHz wideband QPSK transmitter in 65nm CMOS," in *Proc. IEEE Radio Frequency Integrated Circuits Symposium (RFIC) 2014*, June 2014, pp. 353–356.

[12] J. D. Park, S. Kang, S. V. Thyagarajan, E. Alon, and A. M. Niknejad, "A 260 GHz fully integrated CMOS transceiver for wireless chip-to-chip communication," in *Proc. Symposium on VLSI Circuits (VLSIC)*, June 2012, pp. 48–49.

[13] K. Katayama, K. Takano, S. Amakawa, S. Hara, A. Kasamatsu, K. Mizuno, K. Takahashi, T. Yoshida, and M. Fujishima, "20.1 a 300GHz 40nm CMOS transmitter with 32-QAM 17.5Gb/s/ch capability over 6 channels," in *Proc. IEEE International Solid-State Circuits Conference (ISSCC)*, Jan 2016, pp. 342–343.

[14] ——, "A 300 GHz CMOS transmitter with 32-QAM 17.5 Gb/s/ch capability over six channels," *IEEE J. Solid-State Circuits*, vol. 51, no. 12, pp. 3037–3048, Dec 2016.

[15] K. Takano, S. Amakawa, K. Katayama, S. Hara, R. Dong, A. Kasamatsu, I. Hosako, K. Mizuno, K. Takahashi, T. Yoshida, and M. Fujishima, "17.9 a 105Gb/s 300GHz CMOS transmitter," in *Proc. IEEE International Solid-State Circuits Conference (ISSCC)*, Feb 2017, pp. 308–309.

[16] I. F. Akyildiz, J. M. Jornet, and C. Han, "Terahertz band: Next frontier for wireless communications," *Physical Communication*, vol. 12, pp. 16–32, 2014.

[17] S. Forestier, P. Bouysse, R. Quere, A. Mallet, J. M. Nebus, and L. Lapierre, "Joint optimization of the power-added efficiency and the error-vector measurement of 20-GHz phemt amplifier through a new dynamic bias-control method," *IEEE Trans. Microw. Theory Techn.*, vol. 52, no. 4, pp. 1132–1141, April 2004.